energies

MDPI

Article

Non-Salient Brushless Synchronous Generator Main Exciter Design for More Electric Aircraft

Filip Kutt *,†, **Michał Michna** † and **Grzegorz Kostro** †

Faculty of Electrical and Control Engineering, Gdańsk University of Technology, 80-233 Gdańsk, Poland; michal.michna@pg.edu.pl (M.M.); grzegorz.kostro@pg.edu.pl (G.K.)

* Correspondence: filip.kutt@pg.edu.pl; Tel.: +48-58-347-19-39

† These authors contributed equally to this work.

Received: 19 April 2020; Accepted: 26 May 2020; Published: 27 May 2020

Abstract: This paper presents a prototype of high speed brushless synchronous generators (BSG) design for the application in autonomous electric power generation systems (e.g., airplane power grid). Commonly used salient pole field of the main generator part of BSG was replaced with a prototype non-salient pole field. The main objective of the research is an investigation into the advantages and disadvantages of a cylindrical field of the main generator part of BSG over the original salient pole field. The design process of the prototype generator is presented with a focus on the electromagnetic and mechanical finite element method (FEM) analysis. The measurements of prototype and commercial BSG were conducted for the nominal speed of 8 krpm. The advantages and disadvantages of the proposed solution were established based on measurements in load and no-load conditions.

Keywords: autonomous systems; brushless synchronous generator; electric power generation; high speed generator

1. Introduction

Modern commercial planes are designed according to the concept of more electric aircraft (MEA) [1–7]. This concept states that the electric power system in future aircraft should replace pneumatic and hydraulic systems supplied from main turbofan engines. The electrical power system should provide the ability to control the aircraft via electromechanical and electrohydraulic actuators and also provide deicing protection and control the pressurization of the cabin. The high increase in electric power demand is the main result of such an approach. High electric power demand, in turn, requires much more powerful generators to supply it. In addition, an important role of the generator is also the ability to work as a starter to accelerate a turbofan engine [7–10]. The increase in power output of the generator should not affect the volume and weight of the generators in a significant way. One of the obvious directions is the increase in the rotational speed of the machine [11–13]. However, one of the consequences of an increase in rotational speed is a higher centrifugal force acting on the rotor parts and the limitation in the rotor and shaft diameters.

To meet the requirements of the MEA concept considers various types of machines with high power densities defined as the power to weight ratio [7,11–14]. In addition to standard, wound field brushless synchronous generator (BSG), it is also proposed to use a permanent magnet (PM) [15,16], a switched reluctance (SR) [17–19] or an induction (IM) [8,20] machine as a starter-generator for aircraft. Despite the diversity of machine types proposed in research and prototype solutions, the BSG with a wound rotor is still the most often used in commercial aircraft. BSG has been used for decades, so its design is well known, tested and relatively reliable. Among its main advantages are the ability to easily control the voltage at the terminals by changing the excitation field, a simple adjustment system,

the ability to easily reconfigure the system. Unfortunately, standard BSG solutions are characterized by low efficiency (<80%), the maximum speed limit is less than 28 krpm and, consequently, also low power density (about 2.5 kW/kg) [11]. Therefore, research and design works are underway on new, alternative constructions for aircraft generators, including PM, SR, and IM generators [11–14]. These machines are characterized by a simpler rotor design, which allows operation at higher rotational velocity with less maintenance required. Permanent magnet generators achieve the highest power densities in relation to weight (from 3.3 to 8 kW/kg), and high efficiency (up to 95%) [10,11,15,16]. The disadvantage of PM generators is the complex regulation of the excitation field and voltage at the terminals and also the problem with excitation during a short circuit fault. The main advantage of SR generators is a very simple construction of the rotor, and therefore high reliability. SR generators have lower efficiency and lower power density than PM machines; however, it is still better than BSG [17–19]. On the other hand, SR requires complex control systems and algorithms. IM machines are also a prudent alternative, especially in the multiphase, fault-tolerance design [8,20]. Simple and cheap design, proven control systems and algorithms guarantee reliable work required in the aviation industry.

Only proven and reliable solutions can be used in aviation. The use of new solutions and devices for a commercial aircraft requires a time-consuming and expensive design, verification and certification process [21]. Therefore, research is still being carried out to improve the BSG design both in the context of achieving a better power-to-weight ratio and working at higher speeds and frequencies. These requirements can be met when materials, cooling, and mechanical structure would be improved [11].

High requirements regarding the parameters of the aircraft generator can be met by optimizing their design. Therefore, both new construction solutions, as well as new methods of their design, project management and production, are being developed. A wide range of issues related to the design and optimization of electrical machines is of interest to both manufactures and academic centers [14,21–25]. The requirements for high power density and high speed mean that it is important to optimize the generator system as a whole, and not its individual components. The design of the electric machine ceases to be an independent problem, and the optimal solution from the component point of view does not necessarily mean an optimal solution for the entire drive system. The design of the generator system is, therefore, a multi-level, multi-task, multi-disciplinary problem and at the same time nonlinear with many independent variables [26–29].

Computer modelling and simulation methods are widely used in the design process of electrical machines. Optimal use of computer modelling methods and simulations allows one to accelerate design work, verify the importance of potential solutions and, as a result, achieve a product with better parameters. Product development uses both simple analytical methods as well as more complex finite element method (FEM). Obtaining a low mass of the generator can be achieved by increasing the speed or reducing the mass of active materials. High-speed operation requires special attention when designing the rotor. The basis for design should be the selection of appropriate materials and FEM simulations to achieve the expected electromagnetic and mechanical parameters [30]. The reduction of the mass of conductive materials can be achieved by increasing the density of currents. Conducting computational fluid dynamics (CFD) simulation based on a complete conjugate heat transfer (CHT) allows the design of an appropriate cooling system [31].

Even if the final optimization of the machine requires the use of advanced simulation tools (FEM, CFD, etc.), the basis of the project is an analytical method. One of the methods widely used in the pre-design of electric machines is the sizing equation method [32–34].

The brushless synchronous generator is a complex power generation device (Figure 1). Three machines are installed on one shaft: the main generator, the exciter, and the subexciter. Both the main generator and the exciter are electromagnetically excited synchronous generators and the subexciter is a permanent magnet synchronous generator. The main generator field is supplied from the armature winding of the exciter through a 6-phase diode rectifier. The exciter armature is on the rotor along with the field of the main generator and the exciter field winding is on the stator.

The exciter field winding is supplied from the subexciter via a controlled rectifier. The generator control unit (GCU) controls the voltage and the protection systems for the generator. In the variable high-speed operation of the generator, the excitation system is designed to ensure the voltage control (RMS value) requirements of the power grid.

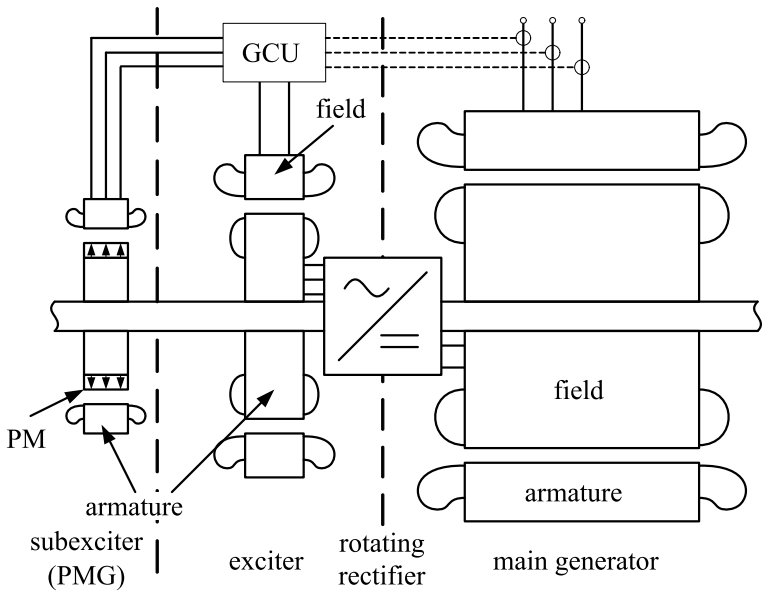

Figure 1. The brushless synchronous generator—based on a three-stage electrical machine topology: the subexciter—permanent magnet generator (PMG); the brushless exciter—synchronous machine with stationary field winding, rotating armature winding and rotating diode rectifier; the main generator—synchronous machine with rotating field winding; GCU—generator control unit.

In modern aircraft such as the Boeing 787 or the Airbus A350XWB the variable frequency generation system is used, where generators are directly driven from the turbofan engines. The system voltage is regulated at 230 V and the bus frequency varies from 350 to 800 Hz. Changing the way in MEA electric power generation requires adaptation of the distribution system and the use of more power electronic converters supplying loads [4]. This affects the power quality, which is also an important issue, as it has a direct effect on the reliability and efficiency of the power system [35]. The harmonic content of produced voltage and current of the main generator can also have a significant influence on the system power quality. In the salient pole machines, the effect of unsymmetrical pole shoe saturation during loaded conditions can increase the harmonic content in induced voltage [36].

2. Objectives and Scope

The main objective of the research is an investigation into the advantages and disadvantages of a cylindrical field of the main generator part of BSG over the original salient pole field. The main motivation for the research was the analysis of the possibility of introducing a cylindrical main filed construction without any detriment to the generated power quality in reference to the original construction. The proposed construction should allow for:

- more sinusoidal back EMF of the generated power due to more sinusoidal excitation winding magneto-motive force (MMF) spatial distribution,
- the possibility of reaching higher rotational velocities of modern MEA variable frequency power systems in future developments of BSG.

The development of a modern aircraft power system is based on MEA concept. However, only repetitively proven and reliable solutions can be used in commercial avionic applications. The MOET FP6 [37] project investigated the component level power system development. The practical

result of the investigation was an evolutional change in the power generation system components and particularly the BSG. The focus of those changes was the improvement of the generator structure for higher efficiency without any detriment to its relatability. That meant the introduction of a variable frequency system with a higher rotational velocity of the generator and improved power quality. The proposal in this paper solution is aiming to investigate the possible advantages in this regard of a cylindrical structure of the main exciter of the BSG. The literature on the subject of the construction of BSG main exciter is very limited and only investigates the possibility of using claw pole design [38] for the main exciter of the machine or the possibility of using a cylindrical structure for operation with higher rotational velocity [39].

The comparative study is conducted on a commercial and redesigned generator construction. Both machines are three stage machines consisting of a permanent magnet generator (PMG) subexciter, an inverted synchronous generator exciter and the main synchronous generator. The only difference between the two machines is the construction of the main generator field (Figure 2). The commercially available machine has a salient pole main generator field construction and the proposed prototype has a cylindrical (non-salient pole) construction of the main generator field. The proposed prototype was designed as a cylindrical rotor machine in order to obtain sinusoidal distributed excitation winding MMF with the possibility of achieving adequate mechanical strength when working at a higher rotational speed. The reverse engineering approach was used on the commercial salient pole generator to determine the electromagnetic parameters of the machine. The generator performance in the steady state was measured and analyzed. The main factor for the analysis was the minimization of the high-order harmonic content of currents and voltages waveforms during the no-load and load operation.

The design of the prototype generator is based on the salient pole brushless synchronous generator type GT40PCz8 ($S_n = 40$ kVA, $U_n = 208$ V, $p.f. = 0.8$, $n_n = 8000$ rpm) used in the Russian MI-28 helicopter and is a typical construction for avionic application. The commercial generator has a salient pole field of the main generator part and the proposed and constructed prototype uses a non-salient pole field (Figure 2).

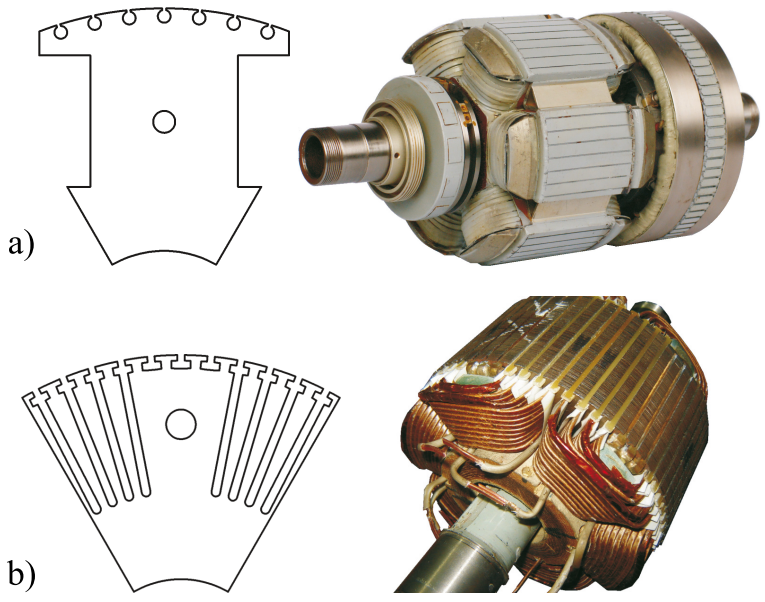

Figure 2. Two types of exciter of the main generator: (**a**) salient pole (original commercial structure, exciter, and subexciter on one shaft); (**b**) non-salient pole (prototype structure, exciter, and subexciter temporally removed from the shaft).

The commercial GT40PCz8 generator was the subject of the reverse engineering process using analytical calculations and FEM simulations. This approach was used to determine the value of

electromagnetic parameters such as current densities in the armature and field windings and magnetic flux density in various parts of the machine. Based on those values, the new main generator field was designed and developed.

The main contribution of the research is the design of the prototype of the main generator part cylindrical exciter that provides better power quality in no-load and under load conditions. This will allow for future developments for variable frequency power system higher maximum frequency.

3. Solution

The development and the implementation of a new design of the electrical machine requires a comprehensive approach to the physical phenomena taking part in the electromechanical energy conversion process in the drive system.

The first step of the design and analysis process is an electric machine design based on analytical calculations (Figure 3). The dimensions of a machine are calculated based on the sizing equations approach [22,34]. The sizing equation describes the relationship between the output power of the machine (P) and its main dimensions design features, material parameters, and rotational speed:

$$P = \frac{\pi}{2} K_I K_P K_E \frac{f_s}{p} (A_s B_m)(D_s^2 l_s) \quad (1)$$

where: f_s—the stator voltage frequency, p—the number of pole pairs; the machine main dimensions: D_s—the inside stator diameter, l_s—the length of stator core; the machine design features: K_I—the current waveform factor, K_P—the electrical power waveform factor, K_E—the EMF (electromotive force or induced voltage) factor which incorporates the winding distribution factor and the air gap magnetic flux distribution, and the material parameters: A_s—the stator electric loading, and B_m—the air gap flux magnitude. The values of the design feature factors depend on the type of the machine, the type of the power supply (shape of the current waveform), the air gap flux distribution and the field and armature winding distributions [22].

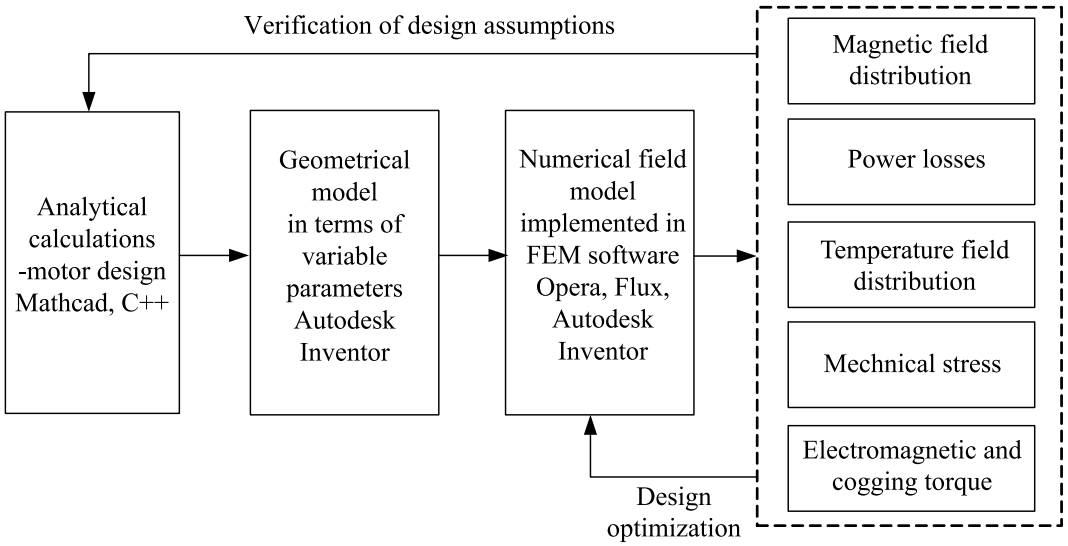

Figure 3. Design process and analysis of the electrical machine—analytical calculation, numerical field model implemented in FEM software.

The main generator stage designed process was conducted based on the sizing Equation (1) and the parameters presented in Table 1. The parameters for the design process were derived from the reverse engineering of the original generator. The design process assumed that the new exciter should allow for the higher rotational speed of the BSG. In addition, the excitation winding should generate a sinusoidal distribution of magnetomotive force (MMF) to generate a sinusoidal distribution of the

air gap flux density. Part of the solution for the proposed assumption was to use a high number of rotor slots. The outer diameter of the original and new field structure of the main generator is $D_r = 173.8$ mm, the airgap length is $\delta = 0.6$ mm and the core length is $l = 73$ mm. The most important difference is that in a salient pole solution the air gap length varies, and, in a non-salient solution, it is constant. An additional advantage of the uniform air gap length is the decrease in non-uniform pole shoe saturation of the field during the under load operation of the BSG.

Table 1. Assumptions for the main generator stage design process.

Parameter	Value	Description
S_n	40 kVA	nominal power
U_s	208 V	nominal voltage
I_s	111 A	nominal current
f_n	400 Hz	nominal frequency
PF_n	0.8	nominal load power factor
$I_f n$	45 A	nominal field winding current
p	3	number of pole pairs
m	3	number of phases
Q_s	81	number of stator slots
Q_r	66	number of rotor slots
N_s	27	number of armature winding turns
δ	0.6 mm	air gap length
D_s	175 mm	inner diameter of the stator
l	73 mm	machine length
b_1	2 mm	stator and rotor slot opening

The prototype field dimensions are partly based on the original generator construction and partly on the selected manufacturing technology, in particular, the technology of field winding construction and manufacturing. In the proposed manufacturing process, a square profile wire was selected for the field winding to maximize the fill factor. The minimum tooth thickness was calculated and then verified using FEM models for the machine to sustain the centrifugal forces and also due to the maximum value of the flux density in the field core. Figure 4 shows the dimensions of the main generator stator and both the commercial and the prototype generator rotors. The original salient pole excitation winding has 42 turns per pole and the design cylindrical prototype has 40 turns per pole. The cross section of the original and prototype excitation winding wire is the same and is equal to 4.5 mm^2.

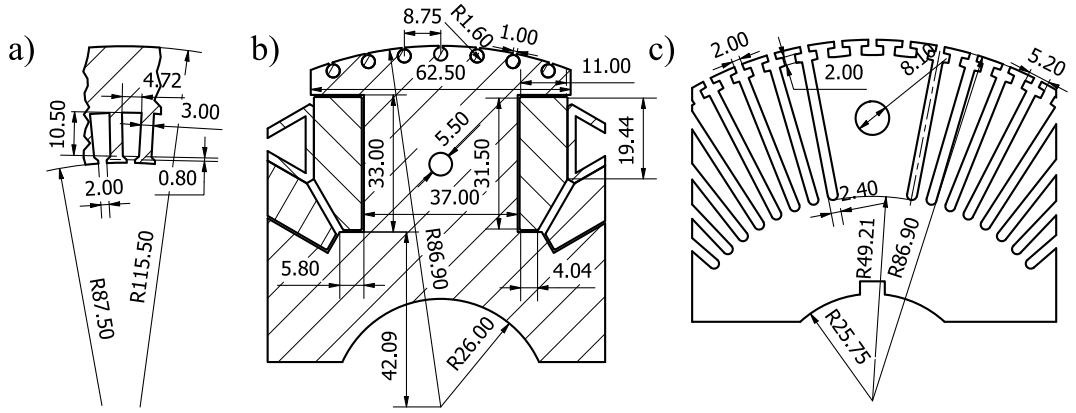

Figure 4. Dimensions of the: (**a**) main generator stator; (**b**) original salient pole rotor; (**c**) prototype non-salient pole rotor.

The proposed design prototype apart from allowing higher rotational velocity of the machine should also decrease the high-order harmonic content of the induced EMF. Both the air gap flux density

spatial distribution and the field and armature winding spatial distribution influence the harmonic content of the induced EMF. To analyze this influence, the air gap length distribution functions and field and armature winding distribution functions have to be defined. The air gap length distribution function is defined as:

$$\delta\left(\phi_s - \theta_r\right) = \frac{1}{\alpha_\delta} \frac{1}{\alpha_0 - \sum\limits_{k=1}^{k_\delta} \alpha_{2k-1} \cos\left(2\left(2k-1\right)\left(\phi_s - \theta_r\right)\right)} \tag{2}$$

where α_δ defines the average length of the air gap, α_0 and α_{2k-1} are the relative components of the air gap length distribution function ($\alpha_0 = 1$), ϕ_s is the angular position along the stator and θ_r is the displacement angle of the rotor axis in reference to the stator axis. In case of the prototype machine with cylindrical stator and rotor, this function is defined as:

$$\delta = \frac{1}{\alpha_\delta} \tag{3}$$

The armature winding distribution is defined based on the winding MMF distribution as:

$$N_{xs}\left(\phi_s\right) = \frac{1}{i_{xs}} \frac{\partial\, MMF_{xs}\left(i_{xs}, \phi_s\right)}{\partial\, \phi_s} \tag{4}$$

where x refers to phase a, b or c in three phase machine, i_{xs} is the x'th phase armature current and the $MMF_{xs}\left(i_{xs}, \phi_s\right)$ is the x'th phase magnetomotive force distribution. This force is defined as:

$$MMF_{xs}\left(i_{xs}, \phi_s\right) = \frac{N_s}{2} i_{xs} \sum_{k=1}^{k_{MMF_s}} A_{s,2k-1} \cos\left(\left(2k-1\right)\left(\phi_s + \theta_{xs}\right)\right) \tag{5}$$

where N_s represents the number of turns of equivalent sinusoidally distributed armature winding, $A_{s,2k-1}$ are the relative amplitudes of armature winding MMF distribution ($A_{s,1} = 1$), θ_{xs} is the angular displacement of x'th phase in reference to phase a ($\theta_{as} = 0$) and k_{MMF_s} is the number of odd harmonics used to approximate the armature MMF distribution. The same winding distribution and magnetomotive force distribution functions can be defined for field winding:

$$N_{fd}\left(\phi_r\right) = \frac{1}{i_{fd}} \frac{\partial\, MMF_{fd}\left(i_{fd}, \phi_r\right)}{\partial\, \phi_r} \tag{6}$$

$$MMF_{fd}\left(i_{fd}, \phi_r\right) = \frac{N_{fd}}{2} i_{fd} \sum_{k=1}^{k_{MMF_{fd}}} A_{fd,2k-1} \sin\left(\left(2k-1\right)\left(\phi_r\right)\right) \tag{7}$$

where i_{fd} is the field current, ϕ_r is the angular position along the rotor, N_{fd} represents the number of turns of the equivalent sinusoidally distributed field winding, $A_{fd,2k-1}$ are the relative amplitudes of field winding MMF distribution ($A_{fd,1} = 1$) and $k_{MMF_{fd}}$ is the number of odd harmonics used to approximate the field MMF distribution. Based on the winding distribution the MMF distribution and the air gap length distribution, one can calculate the mutual inductance between field winding and phase winding:

$$L_{xsfd}(\theta_r) = \frac{1}{i_{fd}} \int_{\pi}^{2\pi} \left(N_{xs}\left(\phi_s\right) \int_{\phi_s}^{\phi_s+\pi} \frac{MMF_{xs}\left(i_{xs}, \phi_s\right)}{\delta(\zeta - \theta_r)} d\zeta \right) d\phi_s \tag{8}$$

If Equations (3), (4) and (7) are applied to relation (8), the function for mutual inductance is defined as:

$$L_{xsfd}(\theta_r) = L_{sfd} \sum_{k=1}^{k_{L_{sfd}}} \left((2k-1)\, \alpha_0 A_{s,2k-1} A_{fd,2k-1} \sin\left((2k-1)\, (\theta_r + \theta_{xs}) \right) \right) \tag{9}$$

where:

$$L_{sfd} = \frac{N_s N_{fd}}{4} \mu_0 l \pi r \alpha_d \tag{10}$$

where μ_0 is the magnetic permeability of vacuum, l is the machine length and r is the distance from the axis of machine to the middle of the air gap. As can be noticed, the mutual inductance harmonic components depend on the air gap length and the armature and field winding distribution high-order harmonics. In the designed prototype, the armature winding was not changed. However, both the air gap length distribution and the field winding distribution were changed. The proposed solution for more sinusoidally distributed excitation winding MMF was to use a high number of rotor slots. Because the prototype has a cylindrical construction and more sinusoidally distributed winding, then the commercial generator the resulting EMF is much more sinusoidal. Figure 5 shows the MMF distribution for both the commercial and the prototype main generator field windings.

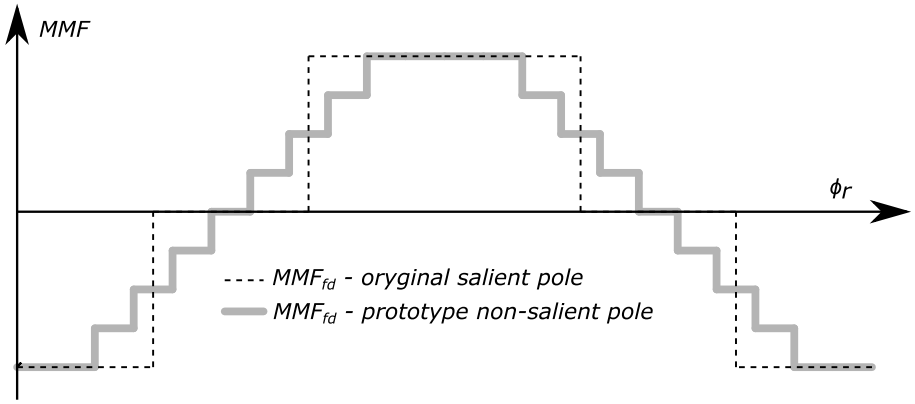

Figure 5. MMF distribution for the commercial and the prototype machine main generator field windings.

Simplified mechanical calculations have been performed to approximate forces and pressures acting on the prototype main generator field core. The force acting on the weakest part of the rotor was calculated as a sum of two forces:

- The centrifugal force acting on rotor tooth—F_{tooth},
- The centrifugal force acting on the winding in the rotor slot F_{Cu}.

The centrifugal force acting on the rotor tooth was calculated as:

$$F_{tooth} = \omega^2 \int_0^c \rho_{Fe} \cdot l \left(a + \left(x \frac{b-a}{c} \right) \right) (r_1 + x)\, dx \tag{11}$$

where ω is the mechanical rotational velocity of the rotor, ρ_{Fe} is the density of rotor core, l is the length of the main generator part of the machine, a is tooth thickness at the bottom of the tooth, b is the tooth

thickness at the top of the tooth, c is the height of the tooth and r_1 is the bottom radius of the rotor tooth. The force acting on the copper in the slot was calculated as:

$$F_{Cu} = \omega^2 \int_0^c \rho_{Cu} \cdot l \cdot d\,(r_1 + x)\,dx \tag{12}$$

where d is the width of the copper profile wire in the rotor slot. The resulting force acting on the rotor tooth from both the tooth itself and the copper in the slot is about 23 kN. The resulting pressure in the thinnest part of the rotor tooth is about 126 MPa.

Because the resulting machine dimensions and the resistance of excitation winding did not change for the prototype and original commercial generator, the thermal analysis of the prototype was not conducted. However, if this solution was to be implemented in a commercial power system, such analysis would have to be conducted.

Three-dimensional (3D) geometric models of the machine are then developed as the parametric model using CAD software. This approach enables easy modification of the geometric models and studying of the influence of the geometrical parameters and material properties on the magnetic field distribution, power losses, integral parameters (inductances, torque), mechanical stresses, etc. (Figure 3).

4. Results

4.1. FEM Simulation

The FEM simulations (using Cedrat/FLUX2D software (version 9.3, Cedrat, Grenoble, France)) have been carried out to verify the designed BSG. Due to a lack of information about the materials used in the commercial generator, the FEM simulations were verified using measurement data. As a result of reverse engineering processes for the given dimensions and measured behavior of the commercial machine, the material parameters of the stator and rotor magnetic core were established. Those parameters were calculated using the iteration process by minimizing the error between measurements of no-load state and FEM simulation results. The initial relative permeability $\mu_r = 8000$ and the magnetic polarization at saturation of 1.6 T parameters were set for the commercial machine stator and rotor core. For the prototype field core of the main generator, M530-50A steel sheets have been used. Unfortunately, the manufacturing process and relatively poor stacking factor caused the necessity for additional varnish coating insulation between steel sheets. During the laser cutting process of the prototype core steel sheets, a slag caused by laser cutter needed to be removed. This process also damaged the original varnish insulation coating on the surface of the steel. Because of this decrease in the stacking factor and the damage done to the cut edge of the electrical steel, the material magnetic characteristic has changed. The field core parameters for the simulation were set to $\mu_r = 500$ (initial relative permeability) and the magnetic polarization at saturation of 1.55 T.

The model was implemented in the Cedrat/FLUX2D software using a dedicated Python script. For the discretization of the FEM model, the air gap was divided into three sections: the stator static mesh section, the rotor moving mesh region and the air gap re-meshing region for the mesh generation during the rotor movement. The resulting mesh and geometry of both the commercial and prototype generator are shown in Figure 6.

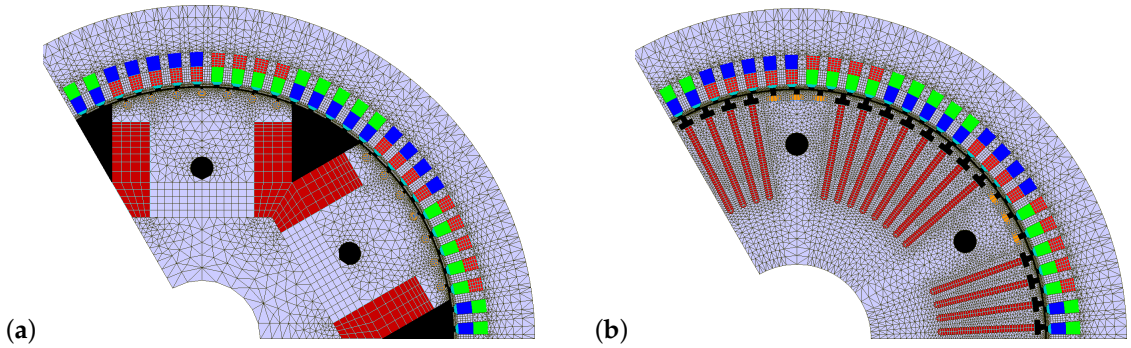

Figure 6. FEM model mesh of the: (**a**) commercial salient pole field BSG; (**b**) prototype cylindrical field BSG.

The resulting mesh generation process led to a total number of about 36 thousand nodes for the original salient pole main generator of BSG and about 53 thousand for the prototype. The simulation process was conducted with set maximum variation between the iterations of integral calculation of less than 0.1%. Table 2 shows the maximum values of magnetic field densities in the crucial parts of the commercial and designed machines.

Table 2. Maximum values of flux density of the main generator part of BSG.

Part of the Magnetic Circuit	Flux Density (T) in Commercial BSG	Flux Density (T) in Prototype BSG
Airgap flux density	0.8	0.8
Stator yoke flux density	1.45	1.46
Stator tooth flux density	1.58	1.6
Rotor yoke flux density	1.05	1.22
Rotor slot/pole flux density	1.66	1.66

FEM simulation results at no-load conditions for the commercial salient-pole and prototype cylindrical generators are shown on Figure 7.

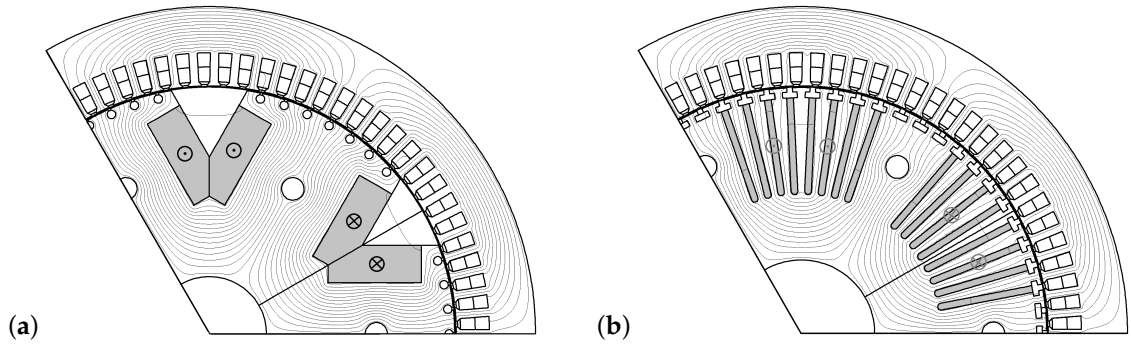

Figure 7. FEM simulation results in no-load conditions: (**a**) commercial salient pole field BSG; (**b**) prototype cylindrical field BSG (marked direction of current in field windings).

The magnetic equipotential lines are shown for both the commercial and the prototype BSG main generator part. In this simulation, the main generator field winding has been supplied with nominal no-load current and FEM computations in magnetostatic conditions have been conducted. The amplitude of the normal component of the air gap flux density of both types of the main generator field has the same maximum value of 0.8 T (Figure 8). The prototype cylindrical generator has got more sinusoidal distribution of air gap flux density (Figure 8).

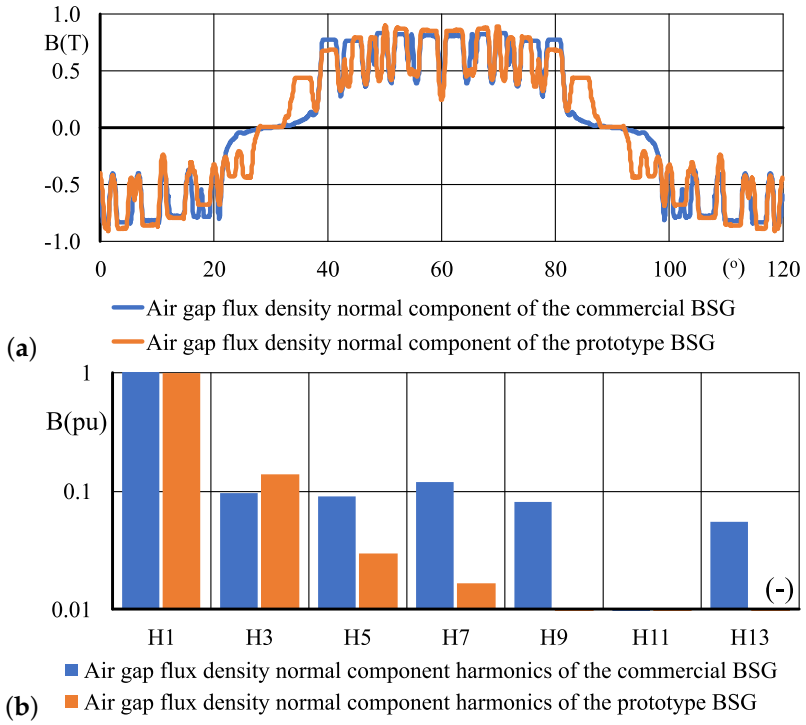

Figure 8. FEM simulation results at no-load conditions—air gap flux density normal component distribution (0.8T—amplitude of the fundamental component): (**a**) commercial salient pole and prototype air gap flux distribution BSG; (**b**) harmonic components of air gap flux distribution.

In addition to electromagnetic calculations, the mechanical calculations concerning the centrifugal forces have been conducted. The simulation of this force acting on one of the rotor teeth was analyzed. The stress analysis module of Autodesk Inventor software (version 2014, Autodesk, San Rafael, CA, USA) was used to perform the mechanical FEM simulation. The rotation speed of 16 krpm has been applied to the rotor. The materials used for stator (steel sheets), windings (copper), and slot wedges (bras) were defined. The stress analysis results are shown in Figure 9. In the simulation, only the copper inside of the slots is considered as the copper in the end windings will not be held by the rotor core itself.

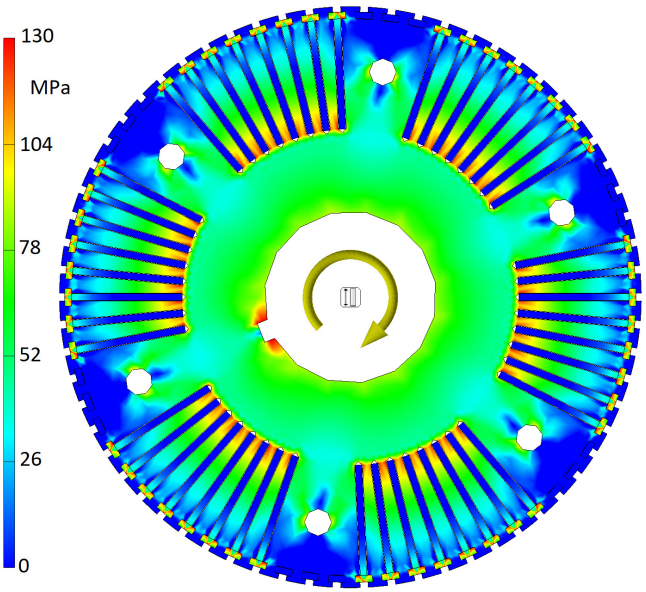

Figure 9. FEM simulation stress analysis results of centrifugal force acting on the rotor.

The electromagnetic and mechanical FEM simulations verified the assumptions and results of the analytical calculations. The proposed solution delivers more sinusoidal distribution of the excitation winding MMF and the maximum tensile stress due to centrifugal force does not exceed maximum tensile stress allowed for M530-50A steel.

4.2. Measurements

Measurements have been carried out for the no-load (open circuit) and load conditions of the prototype and commercial BSG. Measurements of the no-load back EMF in the function of field current for constant speed are shown in Figure 10. This shows that the prototype's main generator field requires more than two times the no-load nominal excitation current. The main factor in this is the smaterial and manufacturing technology used for the core of the main generator field. The difference in number of turns between the prototype and the original machine is only 5% and the air gap length is the same. This also means that the armature reaction of the prototype generator is diminished.

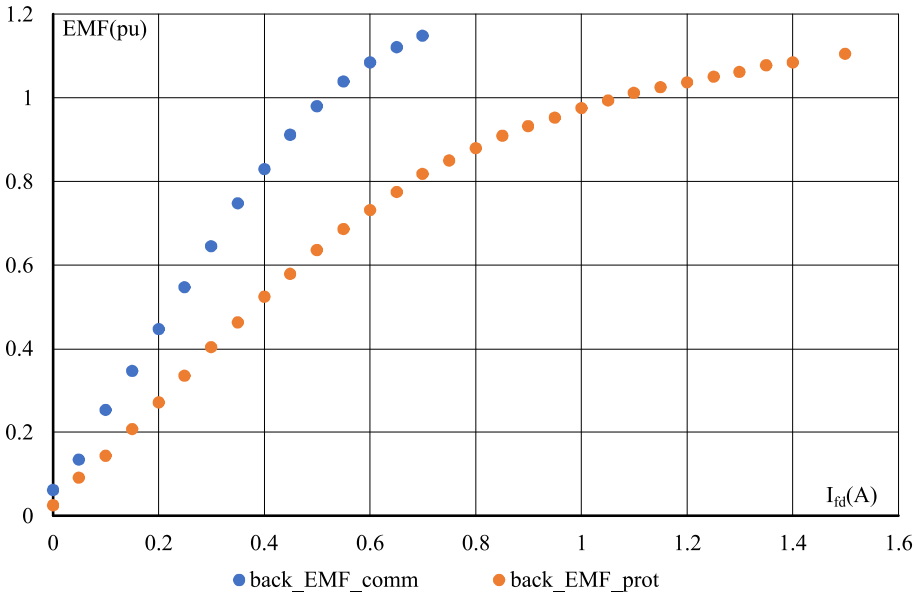

Figure 10. No-load EMF measurements (line to line value) in the function of the exciter field current for commercial generator (back_EMF_comm) and prototype generator (back_EMF_prot).

The no-load back EMF waveform of the prototype has less high-order harmonic components than the commercial one (Figure 11). In both machines, the stator winding is the same which means that the back EMF waveform is dependent on the air gap flux density spatial distribution which in case of a prototype generator is more sinusoidal.

For the load conditions measurements, a load impedance consisting of 0.8 Ω active part and 0.15 Ω reactive inductive part (@400 Hz) has been used. The measurement results of the voltage and current harmonic components in load conditions are shown in Figure 12. As can be observed, the designed prototype with non-salient pole field of the main generator produces less high-order harmonics in the back EMF waveform.

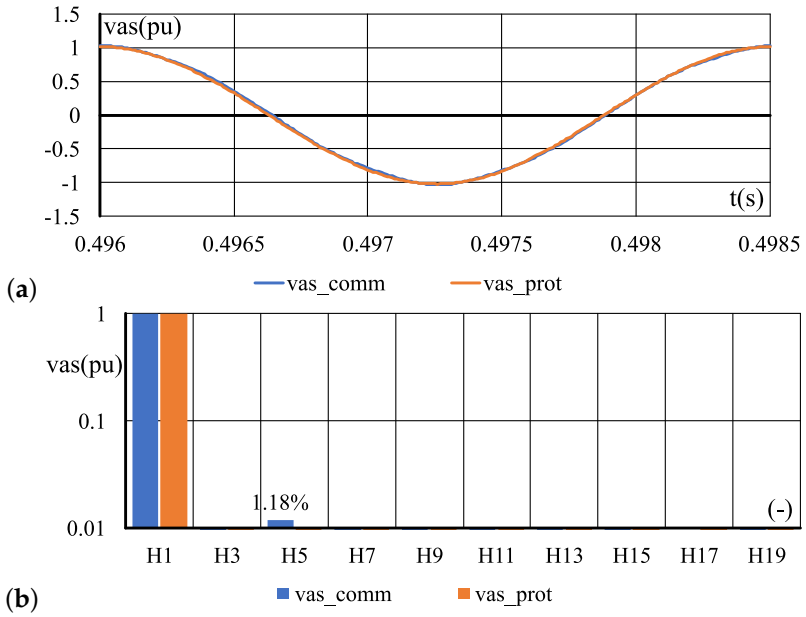

Figure 11. No-load voltage for prototype and commercial BSG: (**a**) back EMF waveform, (**b**) harmonic content of back EMF (vas_prot—measured for prototype BSG, vas_comm—measured for commercial BSG).

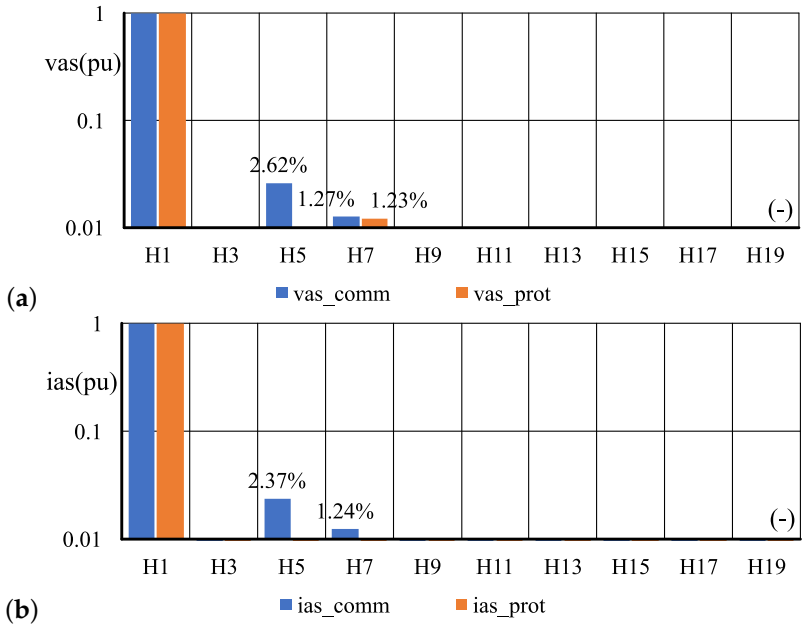

Figure 12. Measurement of armature voltage and current of the salient and non-salient BSG in load conditions (balanced star connected load $R = 0.8\ \Omega$, $X = 0.15\ \Omega$ (@400 Hz), $p.f. = 0.98$), (**a**) harmonic content of voltage waveforms, (**b**) harmonic content of current waveforms (vas_comm, ias_comm—results for salient pole generator, vas_prot, ias_prot—results for non-salient pole generator).

In addition to no-load and under load steady state test, a transient state of the symmetric short circuit was performed (Figure 13). This test was performed by shorting the armature terminals when the machine was operating at no-load condition with the nominal voltage at the terminals. As can be observed, the excitation current is higher in the prototype generator than in the commercial one and equal in steady state to the nominal no-load excitation current.

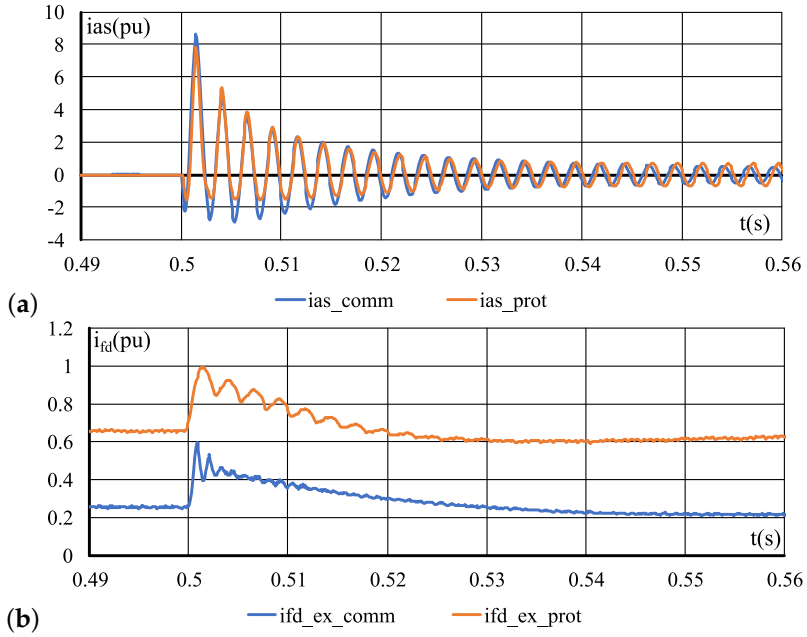

Figure 13. Measurement of armature and exciter currents during transient short circuit test: (**a**) armature currents; (**b**) exciter currents (ias_comm, ifd_ex_comm—results for salient pole generator, ias_prot, ifd_ex_prot—results for non-salient pole generator).

5. Conclusions

The comparative study of two types of BSG main generator exciter has been conducted. The salient pole and cylindrical exciter construction have been compered. The exciter and subexciter of BSG were not changed. The design process was composed of analytical calculation, electromagnetic FEM calculations, and mechanical FEM calculations. The mechanical calculations were conducted to analyze the centrifugal force impact on the designed field of the main generator at higher than nominal (16 krpm while nominal is 8 krpm) rotational velocity, whereas the electromagnetic FEM simulations have been conducted in order to verify the analytically calculated dimensions and parameters of the main generator exciter.

The BSG with the prototype non-salient field has a higher volume and mass of the magnetic core (cylindrical core—9.3 kg, salient pole core—8.1 kg). The volume and mass of the copper used for the field coils are slightly smaller in design and build a prototype (cylindrical field windings copper—2.7 kg, salient pole field windings copper—2.9 kg).

The measurements were conducted at a nominal rotational speed of 8 krpm due to the same exciter and subexciter in both generators. The results of the measurements show significant advantages of the designed solution. Because of more sinusoidal MMF distribution of the field winding, the no-load phase voltage contains less high-order harmonics than the voltage of the silent pole commercial BSG (GT40PCz8). The possibility of operation at higher rotational speeds and better quality of produced electrical energy are a good indicator for the development of the BSG for the MEA variable frequency power system.

The designed generator also has its flaws. It is slightly heavier than the original, and the cooling of the field winding will be different (lack of axial vents in the designed rotor). The selected technique of the manufacturing leaves much to be desired and will have to be modified to archive better magnetic permeability of the field core.

Author Contributions: Conceptualization, F.K., M.M., and G.K.; methodology, F.K. and M.M.; software, F.K. and G.K.; validation, F.K., M.M., and G.K.; formal analysis, M.M.; investigation, G.K.; resources, F.K. and M.M.; writing—original draft preparation, F.K.; writing—review and editing, M.M. and G.K.; visualization, F.K.; supervision, M.M. and G.K.; project administration, F.K.; funding acquisition, F.K. All authors have read and agreed to the published version of the manuscript.

Funding: This research was funded by the Polish Ministry of Science and Higher Education Grant No. N N510 328937.

Conflicts of Interest: The authors declare no conflict of interest.

Abbreviations

The following abbreviations are used in this manuscript:

BSG	Brushless Synchronous Generator
EMF	Electromotive Force
FEM	Finite Element Method
GCU	Generator Control Unit
IM	Induction Machine
MEA	More Electric Aircraft
MMF	Magnetomotive Force
PM	Permanent Magnet
PMG	Permanent Magnet Generator
SR	Switched Reluctance

References

1. Ni, K.; Liu, Y.; Mei, Z.; Wu, T.; Hu, Y.; Wen, H.; Wang, Y. Electrical and Electronic Technologies in More-Electric Aircraft: A Review. *IEEE Access* **2019**, *7*, 76145–76166. [CrossRef]
2. Emadi, K.; Ehsani, M. Aircraft power systems: Technology, state of the art, and future trends. *IEEE Aerosp. Electron. Syst. Mag.* **2000**, *15*, 28–32. [CrossRef]
3. Barzegar, A.; Su, R.; Wen, C.; Rajabpour, L.; Zhang, Y.; Gupta, A.; Gajanayake, C.; Lee, M.Y. Intelligent power allocation and load management of more electric aircraft. In Proceedings of the 2015 IEEE 11th International Conference on Power Electronics and Drive Systems, Sydney, Australia, 9–12 June 2015; pp. 533–538. [CrossRef]
4. Sarlioglu, B.; Morris, C.T. More Electric Aircraft: Review, Challenges, and Opportunities for Commercial Transport Aircraft. *IEEE Trans. Transp. Electrif.* **2015**, *1*, 54–64. [CrossRef]
5. Kim, M.; Lee, S.; Bae, S. Decentralized Power Management for Electrical Power Systems in More Electric Aircrafts. *Electronics* **2018**, *7*, 187. [CrossRef]
6. Chang, J.; Wang, A. New VF-power system architecture and evaluation for future aircraft. *IEEE Trans. Aerosp. Electron. Syst.* **2006**, *42*, 527–539. [CrossRef]
7. Henke, M.; Narjes, G.; Hoffmann, J.; Wohlers, C.; Urbanek, S.; Heister, C.; Steinbrink, J.; Canders, W.R.; Ponick, B. Challenges and Opportunities of Very Light High-Performance Electric Drives for Aviation. *Energies* **2018**, *11*, 344. [CrossRef]
8. Bu, F.; Liu, H.; Huang, W.; Hu, Y.; Degano, M.; Gerada, C.; Rajashekara, K. Induction-Machine-Based Starter/Generator Systems: Techniques, Developments, and Advances. *IEEE Ind. Electron. Mag.* **2020**, *14*, 4–19. [CrossRef]
9. Nøland, J.K.; Leandro, M.; Suul, J.A.; Molinas, M.; Nilssen, R. Electrical Machines and Power Electronics For Starter-Generators in More Electric Aircrafts: A Technology Review. In Proceedings of the IECON 2019—45th Annual Conference of the IEEE Industrial Electronics Society, Lisbon, Portugal, 14–17 October 2019; Volume 1, pp. 6994–7001. [CrossRef]
10. Zhang, Z.; Liu, Y.; Li, J. A HESM-Based Variable Frequency AC Starter-Generator System for Aircraft Applications. *IEEE Trans. Energy Convers.* **2018**, *33*, 1998–2006. [CrossRef]
11. Wang, Y.; Nuzzo, S.; Zhang, H.; Zhao, W.; Gerada, C.; Galea, M. Challenges and Opportunities for Wound Field Synchronous Generators in Future More Electric Aircraft. *IEEE Trans. Transp. Electrif.* **2020**. [CrossRef]
12. Madonna, V.; Giangrande, P.; Galea, M. Electrical Power Generation in Aircraft: Review, Challenges, and Opportunities. *IEEE Trans. Transp. Electrif.* **2018**, *4*, 646–659. [CrossRef]
13. Ganev, E. Selecting the Best Electric Machines for Electrical Power-Generation Systems: High-performance solutions for aerospace More electric architectures. *IEEE Electrif. Mag.* **2014**, *2*, 13–22. [CrossRef]
14. Zhang, Z.; Li, J.; Liu, Y.; Xu, Y.; Yan, Y. Overview and development of variable frequency AC generators for more electric aircraft generation system. *Chin. J. Electr. Eng.* **2017**, *3*, 32–40. [CrossRef]

15. Chen, Y.; Liu, B. Design and Analysis of a Five-Phase Fault-Tolerant Permanent Magnet Synchronous Motor for Aerospace Starter-Generator System. *IEEE Access* **2019**, *7*, 135040–135049. [CrossRef]
16. Zhang, Z.; Huang, J.; Jiang, Y.; Geng, W.; Xu, Y. Overview and analysis of PM starter/generator for aircraft electrical power systems. *CES Trans. Electr. Mach. Syst.* **2017**. [CrossRef]
17. Borg Bartolo, J.; Gerada, C. Design and Modeling of a 45kW, Switched Reluctance Starter-Generator for a Regional Jet Application. In Proceedings of the SAE 2014 Aerospace Systems and Technology Conference, Cincinnati, UK, 23–25 September 2014. [CrossRef]
18. Shoujun, S.; Weiguo, L.; Peitsch, D.; Schaefer, U. Detailed Design of a High Speed Switched Reluctance Starter/Generator for More/All Electric Aircraft. *Chin. J. Aeronaut.* **2010**, *23*, 216–226. [CrossRef]
19. Ferreira, C.A.; Richter, E. Detailed Design of a 250-kW Switched Reluctance Starter/Generator for an Aircraft Engine. *SAE Trans.* **1993**, *102*, 289–300.
20. Liu, H.; Bu, F.; Huang, W.; Liu, L.; Hu, Y.; Degano, M.; Gerada, C. Control Strategy for Five-Phase Dual-Stator Winding Induction Starter/Generator System. *IEEE Trans. Ind. Electron.* **2020**, *67*, 2607–2617. [CrossRef]
21. Galea, M.; Giangrande, P.; Madonna, V.; Buticchi, G. Reliability-Oriented Design of Electrical Machines: The Design Process for Machines' Insulation Systems MUST Evolve. *IEEE Ind. Electron. Mag.* **2020**, *14*, 20–28. [CrossRef]
22. Pyrhonen, J.; Jokinen, T.; Hrabovcová, V. *Design of Rotating Electrical Machines*, 2nd ed.; Wiley: Chichester, UK, 2014.
23. Asfirane, S.; Hlioui, S.; Amara, Y.; Gabsi, M. Study of a Hybrid Excitation Synchronous Machine: Modeling and Experimental Validation. *Math. Comput. Appl.* **2019**, *24*, 34. [CrossRef]
24. Sun, L.; Zhang, Z.; Yu, L.; Gu, X. Development and Analysis of a New Hybrid Excitation Brushless DC Generator With Flux Modulation Effect. *IEEE Trans. Ind. Electron.* **2019**, *66*, 4189–4198. [CrossRef]
25. Gieras, J.F. *Advancements in Electric Machines*; Power Systems; OCLC: 637451957; Springer: Dordrecht, The Netherlands, 2008.
26. Lei, G.; Zhu, J.; Guo, Y. *Multidisciplinary Design Optimization Methods for Electrical Machines and Drive Systems*; Power Systems; Springer: Berlin/Heidelberg, Germany, 2016. [CrossRef]
27. Ounis, H.; Sareni, B.; Roboam, X.; De Andrade, A. Multi-level integrated optimal design for power systems of more electric aircraft. *Math. Comput. Simul.* **2016**, *130*, 223–235. [CrossRef]
28. Amrhein, M.; O'Connell, T.C.; Wells, J.R. An integrated design process for optimized high-performance electrical machines. In Proceedings of the 2013 International Electric Machines Drives Conference, Chicago, IL, USA, 12–15 May 2013; pp. 847–854.
29. Buticchi, G.; Gerada, D.; Alberti, L.; Galea, M.; Wheeler, P.; Bozhko, S.; Peresada, S.; Zhang, H.; Zhang, C.; Gerada, C. Challenges of the Optimization of a High-Speed Induction Machine for Naval Applications. *Energies* **2019**, *12*, 2431. [CrossRef]
30. Shin, K.H.; Bang, T.K.; Cho, H.W.; Choi, J.Y. Design and Analysis of High-Speed Permanent Magnet Synchronous Generator With Rotor Structure Considering Electromechanical Characteristics. *IEEE Trans. Appl. Supercond.* **2020**, *30*, 1–5. [CrossRef]
31. Tosetti, M.; Maggiore, P.; Cavagnino, A.; Vaschetto, S. Conjugate Heat Transfer Analysis of Integrated Brushless Generators for More Electric Engines. *IEEE Trans. Ind. Appl.* **2014**, *50*, 2467–2475. [CrossRef]
32. Huang, S.; Luo, J.; Leonardi, F.; Lipo, T. A general approach to sizing and power density equations for comparison of electrical machines. *IEEE Trans. Ind. Appl.* **1998**, *34*, 92–97. [CrossRef]
33. Moreno, Y.; Almandoz, G.; Egea, A.; Madina, P.; Escalada, A.J. Multi-Physics Tool for Electrical Machine Sizing. *Energies* **2020**, *13*, 1651. [CrossRef]
34. Honsinger, V. Sizing Equations for Electrical Machinery. *IEEE Trans. Energy Convers.* **1987**, *EC-2*, 116–121. [CrossRef]
35. Kutt, F.; Michna, M.; Kostro, G.; Ronkowski, M. Modelling of steady state and transient performance of the synchronous generator considering harmonic distortions caused by non-uniform saturation of the pole shoe. *Electr. Power Syst. Res.* **2017**, *143*, 409–414. [CrossRef]
36. Kutt, F.; Michna, M.; Kostro, G. Multiple Reference Frame Theory in the Synchronous Generator Model Considering Harmonic Distortions Caused by Nonuniform Pole Shoe Saturation. *IEEE Trans. Energy Convers.* **2020**, *35*, 166–173. [CrossRef]

37. More Open Electrical Technologies—TRIMIS—European Commission. 2013. Library Catalog: Trimis.ec.europa.eu. Available online: https://trimis.ec.europa.eu/sites/default/files/project/documents/20121218_094726_85827_MOET_Public_Technical_report.pdf (accessed on 10 May 2020).
38. Arumugam, D.; Logamani, P.; Karuppiah, S. Electromagnetic & thermal analysis of synchronous generator with different rotor structures for aircraft application. *Alex. Eng. J.* **2018**, *57*, 1447–1457. [CrossRef]
39. Biais, F.; Delhasse, F.; Thalin, P. Electrical Power Generation & Start Solutions for the Falcon 5X Program. In Proceedings of the 2015 More Electric Aircraft Conference, Toulouse, France, 3–5 February 2015. Available online: https://www.see.asso.fr/bitcache/91abc2ab86a3f5a69f5b8207260be67011b46135?vid=32132 (accessed on 26 May 2020).